Counter-Rotating Open Rotor (CROR) : flow physics and simulation

Laurence Vion, Grégory Delattre, Fabrice Falissard, Laurent Jacquin

Counter-Rotating Open Rotor (CROR): flow physics and simulation

Laurence Vion[a], Grégory Delattre[b], Fabrice Falissard[c], Laurent Jacquin[d]

a. *Snecma, Rond Point René Raveau, Réau 75550 Moissy-Cramayel*
laurence.vion-ext@onera.fr
b. *Onera - Département d'Aérodynamique Appliquée 8 Rue des Vertugadins 92190 Meudon*
c. *Onera - Département de Simulation Numérique des Ecoulements et Aéroacoustique*
29 Avenue de la Division Leclerc 92322 Châtillon
d. *Onera - Département d'Aérodynamique Fondamentale et Expérimentale 8 Rue des Vertugadins 92190 Meudon*

Résumé :

La propulsion par hélices contrarotatives est à l'étude dans le contexte des recherches menées sur la réduction de la consommation et du bruit aéronautiques. Dans un Open Rotor, on cherche notamment à maîtriser la nappe tourbillonnaire issue de l'hélice amont car elle vient impacter l'hélice aval, contribuant majoritairement au bruit rayonné. Des simulations avancées de ce problème seront présentées et discutées sur le plan de la mécanique des fluides et de l'acoustique.

Abstract:

Counter-rotating open rotor are currently being investigated within the frame of aircraft fuel burn and noise reduction. The vortex sheet shed by the front propeller interacts with the downstream blades, resulting in periodic fluctuations in the aft rotor blades forces. This interaction is a significant noise source and the study of this mechanism is required as a part of the design process for the next generation of open rotor. CFD computations of this problem have been performed and results are discussed from aerodynamic and aeroacoustic points of view.

Mots clefs : **Open Rotor ; Vortex dynamics ; Aeroacoustics**

1 Introduction

Counter-Rotating Open Rotors (CROR) are currently being investigated as a potential alternative to high-bypass turbofan engines, offering the possibility to reduce fuel consumption and CO_2 emissions. They are made of two propellers rotating in opposite direction around the same axis. The upstream propeller induces energy of rotation to the fluid which is recovered by the downstream one, increasing the aerodynamic efficiency.
In the absence of casing, engine manufacturers have to takle the problem of noise generated by such engines in order to meet current international noise rules and to comply with increasingly strict noise requirements.
In the literature, it has been shown that, for some flight conditions such as take-off, the rotor-rotor interaction-driven loading variations are the main noise source [10]. Tip vortex interaction noise occurs when tip vortices, shed from each of the upstream propeller blades, interact with the blades of the downstream propeller. This is particularly critical during take-off and approach because these low-speed conditions require much higher blade loading to attain the required take-off thrust. As a result, tip vortices and wakes are stronger than at the cruise condition. One of the current solution is to reduce the diameter of the aft rotor, so that the tip vortices of the front rotor get over the rear one [9]. But this solution does not suit to take-off, landing and manoeuvre.
The main focus of the present work is on the understanding of the front tip vortices formation and how to reproduce this vortices on a fixed wing.

2 Study of a reference geometry : CROR with HTC5 blade design

2.1 Reference geometry

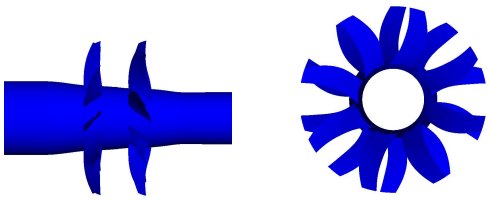

FIG. 1: Counter Rotating Open Rotor HTC5. Left : Side view ; right : rear view

The reference geometry is a CROR with HTC5 blade design which was developed at Onera in the 90's. It is fully defined in [3] and shown in figure 1. This 10×8-bladed pusher-configuration is studied at take-off condition. For the need of the study, this engine was rescaled keeping the advance ratio and the tip Mach number constant. The main characteristics of the engine are :

- Blade number : front : 10 ; rear : 8
- No clipping ; blade radius : $R_{tip} = 0{,}85\,\text{m}$
- Rotor-rotor space : $0{,}45 \times R_{tip}$
- Take-off condition : $M = 0{,}2$
- Advanced ratio $\gamma = 0{,}96$
- Efficiency $\eta = 0{,}62$
- Power coefficient $\chi = 1{,}92$
- Rotational speed for upstream and downstream propeller : 2535 rpm
- Tip Mach number $M_{tip} = 0{,}68$
- Thrust coefficient $\tau = 1{,}24$ (Thrust : 25 000 N)
- Isolated configuration (no pylon, no airframe components,...)
- Infinite cylindrical hub : $R = 0{,}3995\,\text{m}$ upstream and $R = 0{,}2805\,\text{m}$ downstream.
- Reynolds number for a profil at a relative radius 0,7 : $Re_{0,7} = 4,6 \times 10^6$

Thereafter, most results are without dimension after normalization by : the circulation $\Gamma_0 = c_{tip} \times W_{tip}$, the vorticity $\omega_0 = \frac{W_{tip}}{c_{tip}}$, $Q_0 = \left(\frac{W_{tip}}{c_{tip}}\right)^2$ with $c_{tip} = 0,17425\ m$ the tip chord length and W_{tip} the relative velocity at blade tip $W_{tip} = \sqrt{U_\infty^2 + (R_{tip}.\Omega)^2} \approx 236\,m/s$.

2.2 Computational strategy

Recent researchs at Onera, which is currently involved in projects dealing with the optimization and assessment of the aerodynamic and aeroacoustic fields of CROR configuration [8][2][4], have enabled the development of tools for CROR applications, which are succesfully applied. The choosen computational strategy, meshing and numerical parameters lies on Onera experience.

Unsteady 3D RANS simulations were used to determine the time varying blade pressures and insteady flow features necessary to define the acoustic source terms.

2.2.1 Methods Overview

The CFD computations are performed using the Onera 3D *elsA* code.
First, a steady RANS computation is performed using a mixing plane interface between the two rotors. In this approach, each fluid zone is solved as a steady-state problem and the flow datas at the mixing plane interface are averaged in the circumferential direction on both front rotor outlet and rear rotor inlet. The resulting solution provides reasonable approximations of the time-averaged flow-field and is used as initial solution for the unsteady RANS computation. This latter is based on the chorochronic approach, which uses time lagged periodic boundary condition.

The numerical parameters were chosen based on Onera experience for CROR computations[2]. Spatial discretization of the convective fluxes is done using a Jameson centred scheme with artificial dissipation (coefficient for second order 0,5 and for fourth order 0,016)[7] while the viscous fluxes are discretized with scalar upwind method by LU-RELAX relaxation and time with backward Euler discretization. Turbulence in these fully turbulent simulations is modeled by the k-ω model with SST correction and Zeng limiter.

The sound propagation in the farfield is calculated using the Onera KIM code[11], which computes the Ffowcs-Williams/Hawkings (FW-H) equation formulated for solid or porous surfaces as well as the Kirchhoff formulation[5]. In this study, the acoustic prediction lies on the computation of the solid surface formulation of the FW-H equation using unsteady blade pressure distribution provided by the CFD. This method does not account for non-linear propagation effects between the two propellers, but provides some insight with respect to noise source localization. The noise radiated by each rotor is computed separately and the acoustics signals of each propeller are sum up to obtain the actual sound of the CROR at observer location.

2.2.2 Computational Grid and Boundary Conditions

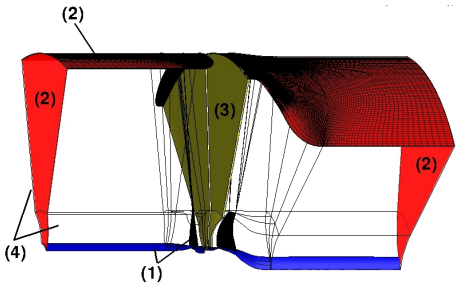

FIG. 2: Computational grid and boundary conditions : (1) solid surface with no-slip condition ; (2) characteristic inflow/outflow boundary conditions based on farfield state ; (3) mixing plane between front and rear propellers (steady computation) or chorochronic plane (unsteady computation) ; (4) periodic boundary condition (steady computation) or chorochronic boundary condition (unsteady computation)

A methodology for mesh generation of Open Rotor was developed and successfully applied at Onera, using the mesh generation tool Autogrid.
The chorochronic asumption allows the use of a single channel domain, thus reducing the CPU time consumption.
The computational grid comprises a total number of 5 680 100 nodes (Front propeller : 2 587 948 nodes ; rear propeller : 3 092 962 nodes). A topology with O4H type grids around the profil and H type grid for the interior passage is used. The blade grid topology (O4H) was extended all the way to the farfield boundary to assure a continuous matching grid. The outer radius of the computation domain is located at 3 blade radius.
The complete setup in terms of boundary conditions is shown in figure 2.

2.3 Aerodynamic and aeroacoustic analysis

2.3.1 Characterisation of the front tip vortices

The CFD computation was made for a single passage according to the chorochronic approach. The entire flowfield was reconstructed thanks to the software Zeppelin, an *elsA* external module for unsteady computations developed at Onera, and is shown in figure 3.

[1] $u_{i,j} = \frac{\partial u_i}{\partial x_j}$

Tip vortices are visualised with Q-criteria isovalue, with Q the second invariant of the velocity gradient tensor.

$$Q = \frac{1}{2}\left(\|\mathbf{\Omega}\|^2 - \|\mathbf{S}\|^2\right)$$

with $\mathbf{\Omega}$ and $\mathbf{S}$ the symmetric and antisymmetric components of the velocity gradient. $S_{ij} = \frac{1}{2}(u_{i,j} + u_{j,i})$ and $\Omega_{ij} = \frac{1}{2}(u_{i,j} - u_{j,i})$ [1]. $\|\mathbf{S}\| = [tr(\mathbf{S}\mathbf{S}^\mathbf{t})]^{1/2}$ and $\|\mathbf{\Omega}\| = [tr(\mathbf{\Omega}\mathbf{\Omega}^\mathbf{t})]^{1/2}$
Hunt and al. [6] define a vortex as a spatial region where Q is positive and the pressure is lower than the ambient value. Q represents the local balance between shear strain and vorticity magnitude.

Figure 3 shows the front tip vortices impinging the rear blades.

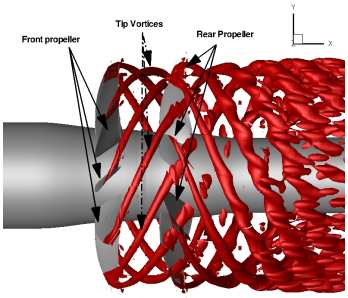

FIG. 3: Iso-Q-criteria to visualize the tip vortices. $Q = 1$. Iso-surfaces for a radius lower than 0,75 are hidden for a better visualization of the tip vortices.

2.3.2 Aeroacoustic results

The sound pressure level obtained in the farfield for a line of virtual microphones parallel to the axis of the engine (x axis) at around 50 R_{tip} are displayed in figure 4. The center of the microphones array is located at the center of the front rotor, the rear rotor is situated at $x = 0,48\,m$.
The CROR features the characterictics known for the single rotation propeller : the blade passing frequencies BPF1 (front rotor) et BPF2 (rear rotor) correspond to the noise of the rotors if alone. But additional noise is generated by the aerodynamic interferences between the two rotor fields : the interaction tones whose frequencies are composed by a combination of the blade passing frequencies (nBPF1+mBPF2 with n and m integers).
The blade passing frequencies dominate in the plane of rotation of the propellers, but for all the other directivities, the noise level spectrum is strongly influenced by the interaction tones.

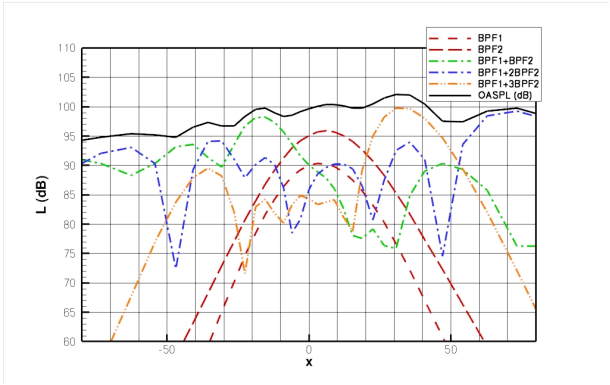

FIG. 4: Overall sound pressure level and tones directivities of the HTC5 CROR at take-off conditions

2.4 Tip vortex

2.4.1 Vortex formation over the blade

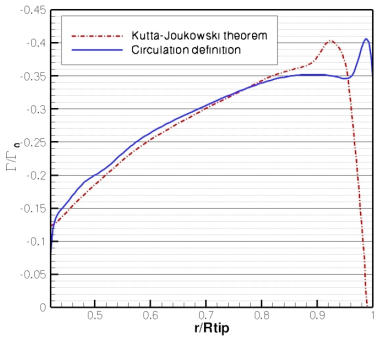

FIG. 5: Circulation distribution along the blade span. Comparison of methods : line integral of the fluid velocity along a closed contour following the streamlines in the moving frame (blue) and Kutta-Joukowski theorem (red).

The wall streamlines on suction side give informations about the formation of the vortex over the wing. Figure 9 left shows a separation line starting at about 35% of the leading edge of the outside blade radius, just beyond the position of maximum forward sweep, and running alongside of the leading-edge. This is characteristic of a leading edge vortex, which leaves the blade before the tip blade. Thanks to this leading edge separation, the leading-edge vortex rolls up and induces low pressure on the upper surface of the blade, resulting in higher lift, the so-called vortex-lift.
For a better understanding of the dynamic of the vortex sheet, a study was carried out to determinate the circulation distribution over the blade. Several methods were adressed and two of them seem to be a good approximation : the line integral of the fluid velocity along a closed contour following the streamlines in the moving frame and the Kutta-Joukowski theorem. The weaknesses of these methods are respectively : - the tip vortex crosses the closed contour and has an identified impact on the circulation distribution (a strong peak of circulation near the tip of the blade) - and the induced velocities are partially neglected. The circulation distributions found with these methods are shown in figure 5. The change in gradient sign of the curve indicates a vortex sheet vorticity the sign of which is opposite of the tip vortex one. Such a circulation distribution is typical of rotating wings.

2.4.2 Vortex formation behind the blade

The flow downstream of the front propeller trailing edge is studied by measuring the flow field in five planes perpendicular to the streakline of the leading-edge vortex. Figure 6 shows a strong tip vortex with negative vorticity and nearby a red spot corresponding to a counter-rotating vortex. At the trailing edge of the blade, free vortices are shed the rotation of which is opposite to that of the leading-edge vortex (change in gradient sign of the circulation distribution curve). The trailing-edge vortex is originally connected to the trailing vortex sheet. When the leading-edge vortex leaves the blade trailing-edge, it interacts with the vortex sheet, which is thus warped and gives birth to a concentrated trailing-edge vortex. This one is embedded in the flow field of the dominant leading-edge vortex. The latter induces velocities at the trailing vortex which lead to an helical path of the trailing vortex around the leading-edge vortex.

For a quantitative view, the focus is made at a position 3 tip chords downstream of the blade along the streakline of one of the front tip vortices. The formula $\Gamma = \iint \vec{\omega}.\vec{ds}$ gives the total circulation with a surface chosen perpendicular to the streakline. $\Gamma^+ = \iint_{\omega>0} \vec{\omega}.\vec{ds}$ gives the circulation of the counter-rotating vortex for a surface which borders does not take into account the vortex sheet, and $\Gamma^- = \iint_{\omega<0} \vec{\omega}.\vec{ds}$ the circulation of the leading-edge vortex.
For the entire sheet, $\frac{\Gamma}{\Gamma_0} = -0,14$, which is the value at the hub for the circulation distribution (figure 5), $\frac{\Gamma^-}{\Gamma_0} = -0,38565$ and $\frac{\Gamma^+}{\Gamma_0} = 0,03193$.

We notice that $\frac{\Gamma^+ + \Gamma^-}{\Gamma_0} = -0.35372$, which is the minimum of the circulation distribution (the peak of the curve represents the vortex contribution and is not representative of the circulation of the blade).

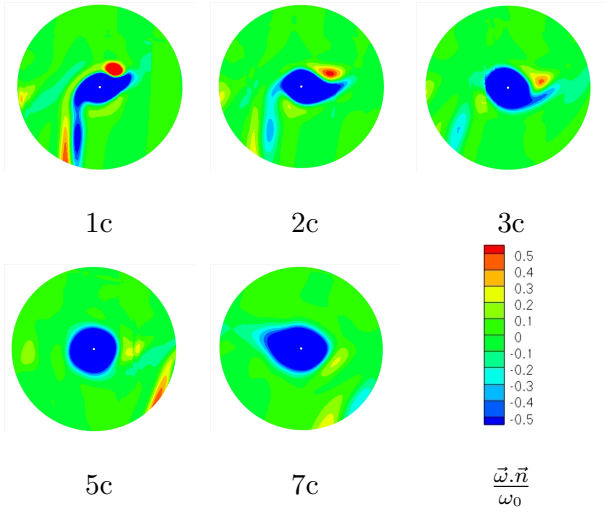

FIG. 6: vorticity normal to streakline for different ages of the vortex

3 Fixed model of rotating blade

The objective of this part is to define a fixed wing geometry which has the same vortex sheet characteristics as a front propeller blade (this fixed wing will be the object of an experiment at the Onera S2L wind tunnel in Meudon in future work). This processus lies on the reproduction of the blade circulation distribution over a fixed wing : the geometry of the blade (sweep angle, chord laws) is maintained but the twist law is modified until the desired repartition is found. Many authors worked on the relationship between tip vortex characteristics and wing lift distribution, including fixed wing [13][12] and rotating blade [1].

The fixed wing results are normalized by the same parameters as the rotating blade ones with $W_{tip} = 38\,m/s$.
Computations aiming at reproducing a fixed wing in a wind tunnel have been performed. For sake of rapidity, the tools used before for CROR were adapted to the fixed wing 3D RANS computations. The aft propeller is removed, the hub radius is enhanced to $6,323\,m$ to approximate a planar hub, the blade number to 98 blades (the localisation of the neighbouring blades corresponds to the wind tunnel walls), the rotor is now fixed and the upstream flow velocity has been lowered to $38\,m/s$ to meet the nominal velocity of the S2L wind tunnel, where the experiments will be conducted. This corresponds to a Reynolds number equal to $Re_{c_{tip}} = 3,6 \times 10^5$.
The Autogrid generated mesh comprises 5 790 730 nodes and has the same topology as the rotating blade one.

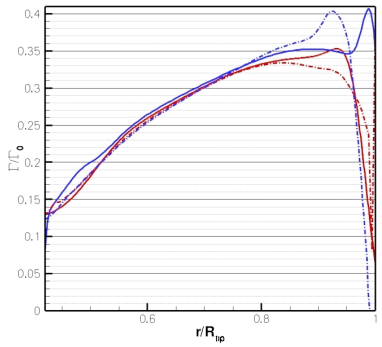

FIG. 7: Comparison of the circulation distribution of the fixed wing (red) and the rotating wing (blue) for the two methods : line integral over a closed contour (solid line) and Kutta-Joukowski theorem (dash-dot line)

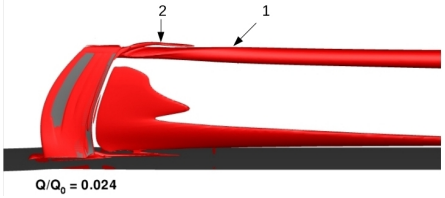

FIG. 8: Iso-Q-criteria surfaces to visualise tip vortices $\frac{Q}{Q_0} = 0,024$

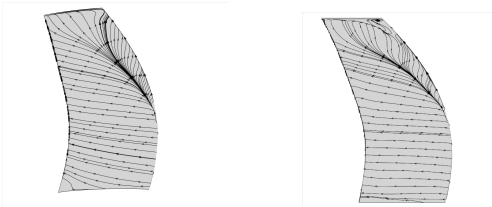

front propeller fixed wing

FIG. 9: wall streamline on suction side

An empirical investigation makes it possible to determinate a blade twist law giving a the circulation distribution close to that of the rotating wing, as shown in figure 7. The curves overlay between $\frac{r}{R_{tip}} = 0,5$ and $\frac{r}{R_{tip}} = 0,75$, parts at hub and tip beeing influenced by vortices.
The visualization of the tip vortices with Q-criteria iso-value (figure 8) clearly shows the presence of two vortices (1 and 2), one (2) wrapping around the other (1).
Comparing qualitatively the wall streamlines on suction side (figures 9) and vorticity normal to the

streakline for different ages (figure 6 and 10), the two configurations look quite similar.

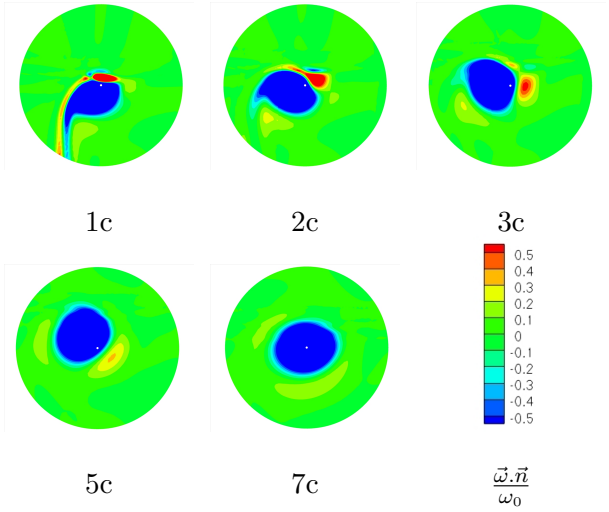

FIG. 10: vorticity normal to the streakline for different ages of the vortex for the fixed wing

The quantitative analysis is resumed in table 3, with the deviation $\frac{X_{fixed}-X_{rotating}}{X_{rotating}} \times 100$, b the distance between the two vortices centers and a the vortex radius, defined as the vorticity dispersion radius, according to the formula :

$$\Gamma = \iint \vec{\omega}.\vec{ds}$$

$$\vec{x_c} = (xc, yc, zc)^T = \frac{1}{\Gamma} \iint \Omega_s \vec{x} dS$$

$$a = \sqrt{\frac{1}{\Gamma} \iint ((x-x_c)^2+(y-y_c)^2+(z-z_c)^2)\Omega_s dS}$$

X	rotating blade	fixed wing	deviation
$\frac{\Gamma^-}{\Gamma_0}$	-0,38565	-0,38921	0,92 %
a^-	0,02910	0,02930	0,7 %
$\frac{\Gamma^+}{\Gamma_0}$	0,03193	0,05204	63,0 %
a^+	0,01512	0,01761	16,5 %
b	0,059469	0,06467	8,7 %

TAB. 1: Comparison of tip vortices parameters at 3 tip chord lengths

The vortices parameters differences are quite small, except for the trailing-edge vortex circulation $\frac{\Gamma^+}{\Gamma_0}$. This should be explain by a root vortex found in the CROR computation but not in that of the fixed wing. The root vortex enables to drain off a part of the positive vorticity. We expect to find this root vortex during the wind tunnel experiment.

4 Conclusions

Numerical investigations based on the Onera know-how were performed to evaluate the aerodynamic and aeroacoustic fields of a given CROR configuration. This first part of the study enabled a better understanding of the vortex sheet development behind a front propeller blade. The vortex sheet is composed of a leading-edge vortex, a contra-rotating trailing vortex and a vortex sheet the vorticity of which is opposed to that of the leading-edge vortex. This vortex system impinges the aft propeller, resulting in additional noise particularly critical during take-offs and landings.
The on-going study deals with the close reproduction of the rotating front blade characteristics on a fixed wing, the geometry of which is based on a change in the rotating blade twist law. A numerical investigation allowed to determinate a fixed wing with the same circulation distribution over the wing. The fixed wing vortex system presents good agreements with the system of the rotating blade. The next step will be an experimental validation at the Onera wing tunnel S2L in Meudon.

Références

[1] Bhagwat, M.J., Leishman, J.G. 2000 Measurement of bound and wake circulation on helicopter rotor *Journal of Aircraft* 37(2) : 227-234, March-April

[2] Boisard, R., Delattre, G., Falissard, F. 2011 Assessment of aerodynamics and aero-acoustics tools for open rotors *European Turbomachinery Conference* March 21-25, Istanbul, Turkey

[3] Bousquet, J.M., Gardarein, P., Gouyon, B., Tichtinsky, J.C. 1991 Définition aérodynamique de l'hélice contrarotative HTC5. Etude et réalisation d'une balance de paroi pour essais hélices dans la soufflerie S3ch. *Technical report, Onera*

[4] Delattre, G., Schnell, R.2011 Cross-comparison of aerodynamic and Acoustic predictions for open rotors with Onera (*elsA*-KIM) and DLR (TRACE-APSIM) codes *Onera-DLR Aerospace Symposium* February 9-11, Toulouse, france

[5] Ffowcs Williams, J., Hawkings, D. 1969 Sound generation by turbulence and surfaces in arbitrary motion *Philosophical transactions of the Royal Society* Vol. A264, pp. 321-342

[6] Hunt, J.C.R., Wray, A.A., Moin, P. 1988 Eddies, stream and convergence zones in turbulent flows *Technical Report CTR-S88, Center for turbulence research Report*

[7] Jameson, A.1991 Time dependant calculations using multigrid, with applications to unsteady flows past airfoils and wings *AIAA Paper 91-1596*

[8] Lepot, I., Leborgne, M., Schnell, R., Yin, J., Delattre, G., Falissard, F., Talbotec, J. 2011 Aero-mechanical optimization of a contra-rotating open rotor and assessment of its aerodynamic and acoustic characteristics *European Turbomachinery Conference* March 21-25, Istanbul, Turkey

[9] Majjigi, R.K., Uenishi, K., Gliebe, P.R. 1989 An investigation of counterrotating tip vortex interaction *NASA Report 185135*

[10] Peters, A., Spakovszky, Z.S. 2010 Rotor interaction noise in counter-rotating propfan propulsion systems *Proceedings of ASME Turbo Expo 2010 : Power for Land, Sea and Air, GT2010-22554* June 14-18, Glasgow, UK

[11] Prieur, J., Rahier, G. 1998 Comparison of Ffowcs Williams-Hawkings and Kirchhoff rotor noise calculations *AIAA Paper 98-2376*

[12] Rossow, V.J. 1973 On the inviscid rolled-up structure of lift-generated vortices *Technical report NASA TM X-62-224*

[13] Rule, J.A., Bliss, D.B. 1988 Prediction of viscous trailing vortex structure from basic loading parameters *AIAA Journal* 36(2) : 208-218, February